Strong impact of the recent Highly Pathogenic Avian Influenza panzootic on population dynamics of a long-lived bird

Jaume A. Badia-Boher[1*], Michael Schaub[1], Martin Mollet[2], Peter van Geneijgen[2], Henk P. van der Jeugd[3,4], Valentina Caliendo[5], Marc Kéry[1]

[1]Population Biology Research Unit, Swiss Ornithological Institute, Sempach, Switzerland

[2]Werkgroep Roofvogels Nederland, the Netherlands

[3]Department of Animal Ecology, Netherlands Institute of Ecology (NIOO-KNAW), Wageningen, the Netherlands

[4]Vogeltrekstation-Dutch Centre for Avian Migration and Demography (NIOO-KNAW), Wageningen, the Netherlands

[5]Dutch Wildlife Health Centre, Utrecht University, Utrecht, the Netherlands

[*]Corresponding author: jaume.badia@vogelwarte.ch

Abstract

Since 2020, the spread of a new Highly Pathogenic Avian Influenza virus (HPAIV-H5N1) has triggered the most severe wildlife panzootic ever recorded, with suspected population crashes in hundreds of species. Yet, no study has evaluated the demographic mechanisms underlying these declines. We used Integrated Population Models and population forecasts to evaluate the demographic impact of HPAIV-H5N1 on a long-lived species population, the peregrine falcon in the Netherlands. We found drastic declines in adult survival – the key driver of population dynamics in long-lived species – along with a sudden ~25% decline in breeding pairs over consecutive panzootic years. Population projections predict recovery to pre-panzootic levels not before 2030. Our findings illustrate how the new HPAIV panzootic can generate unprecedentedly strong, long-lasting population impacts in long-lived species. This raises major concerns about the viability of the many species affected by the panzootic and calls for a global-scale conservation response.

Keywords: Avian Influenza, Integrated Population Modelling, Wildlife Disease, Demographic Analysis, Demographic Resilience, Long-lived Species, Capture-Mark-Recapture, Wildlife Epizootics, Population Models, Peregrine Falcon

Introduction

Infectious wildlife diseases are among the most important causes of population declines and extinctions, and both their frequency and geographic range are predicted to increase due to global change (Daszak et al., 2000; Dobson & Foufopoulos, 2001). A paradigmatic example is the Highly Pathogenic Avian Influenza virus (HPAIV). During the past three decades, HPAIV has spread from poultry to wildlife causing outbreaks in wild birds (Shi et al., 2023). From 2020, a virus of strain H5N1 has caused the most widespread, virulent, and persistent HPAIV panzootic ever recorded (Campagna et al., 2024; Klaassen & Wille, 2023; Lambertucci et al., 2025). For the first time ever, this panzootic has caused severe outbreaks with high-mortality events in all continents except for Oceania, and the death toll among wild vertebrates probably goes into the millions. By 2024, outbreaks were recorded in at least 406 bird and 51 mammal species in the wild (Lambertucci et al., 2025; Plaza et al., 2024a; Pohlmann et al., 2023).

Of particular concern are the effects of HPAIV-H5N1 outbreaks in long-lived species, i.e., species with long life expectancy, delayed sexual maturity, and reduced brood sizes. To sustain viable populations, these species typically rely on high survival probabilities that must be fairly stable over time, and they show only limited recovery ability to perturbations affecting their demography (Capdevila et al., 2022). Reports of mortality in long-lived species due to HPAIV-H5N1 between 2020 and 2023 have been unprecedentedly frequent and widespread. These include, among others, 25,000 Cape cormorants found dead in South Africa (Klaassen & Wille, 2023; Molini et al., 2023), 2700 dead Humboldt penguins in Chile (Muñoz et al., 2024), 25,000 sea lions in South America (Plaza et al., 2024b), 17,000 southern elephant seal pups in Argentina (Campagna et al., 2024), and a full 21 California condors, representing 6% of their world population (Kozlov, 2023).

Importantly, practically all information to date on the population effects of HPAIV is based on counts of animals reported dead (Günther et al., 2024; Rayment et al., 2025). However, we lack a more mechanistic understanding of the precise demographic pathways underlying these population crashes. Intuitively, survival must have declined, but nothing is known about the magnitude of such a decline at the population level nor about its rate over time. Seemingly, little is known about potential HPAIV-induced effects on other vital rates, about whether specific population stages may be more affected than others, and how all of this may affect the overall dynamics of populations and their likely trajectories in the future. As a result of these knowledge gaps, we may currently lack the ability to design and implement effective conservation strategies, i.e., those that target the most affected population stages and most influential demographic parameters. Hence, there is an urgent need for a much deeper understanding of the demographic effects of the recent HPAIV-H5N1 panzootic.

Likewise, the resilience of natural populations to periodic disturbances induced by HPAIV has apparently never been studied. Long-lived species generally show only a limited ability to recover from severe reductions of population size, and need long recovery times (Capdevila, et al., 2022a). As a result, their populations may be at a higher risk for decline if epizootics occur repeatedly within a short time interval (Capdevila et al., 2022b). Furthermore, populations repeatedly affected by strong disturbances may experience an inertial effect on long-term population size. That is, they may stabilize at some level below the carrying capacity in the absence of such disturbances ("population inertia", Koons et al., 2007). Hitherto, it seems that these mechanisms have typically been ignored when trying to understand the effects of severe disturbance in a population, yet they may be essential in the face of the current global increase in the magnitude and frequency of severe disturbances such as epizootics.

Here, we evaluate the precise demographic pathways of the impact of the HPAIV panzootic (2020-2024) on the dynamics and resilience of a long-lived species known to be strongly affected (Caliendo et al. 2024, 2025), the peregrine falcon *Falco peregrinus* in the Netherlands. The study area lies at the crossroads of Western Europe and Scandinavia, and is an area with a particularly high incidence of the HPAIV-H5N1 virus that is known to have caused severe casualties in several bird species (Caliendo et al., 2024). In the Netherlands, population declines, large recorded casualties, and a very high prevalence of positive HPAIV tests in dead peregrine falcons (ca. 80%) suggest a strong impact of recurrent HPAIV outbreaks on this species (Caliendo et al., 2024, 2025). Severe declines have also been reported in some other northern European populations, especially in the Nordic countries (e.g., Järås, 2023; Sundvall, 2024). We analysed Dutch peregrine population dynamics using Integrated Population Models (IPMs), a statistical framework that allows the integration of multiple data streams to jointly estimate demographic parameters (Besbeas et al., 2002; Schaub & Kéry, 2022). Our analyses yield annual estimates of age-specific survival probabilities, productivity, immigration rate, and age- and stage-specific population sizes. In a first step, we evaluate and compare annual fluctuations in parameter estimates before (1993-2020) and during (2020-2024) the most recent HPAIV panzootic. In a second step, we use Bayesian population forecasting to assess two key components of population resilience: recovery time and population inertia (Figure 1; Capdevila et al., 2020). Our results will be relevant for developing effective management strategies that target the most impacted demographic parameters and population stages by HPAIV of this and other long-lived species affected. In addition, we suggest that the accurate demographic accounting yielded by an IPM may become the gold-standard for gauging the effects on a population of a zoonotic or indeed of any other impact.

Methods

Study species and area

The peregrine falcon is a medium-sized territorial raptor which occurs widely in all continents except Antarctica (Ratcliffe, 1993). In Europe, peregrines typically nest in cliffs or on tall buildings, while in our Dutch study area, they use almost exclusively buildings and transmission line poles equipped with nest-boxes (van Geneijgen, 2014). Here, peregrines lay 3-4 eggs in March that hatch after 30 days of incubation. Nestlings fledge around 42 days of age in May and early June (van Meerendonk, 2023). As in many territorial species, young peregrines show a non-territorial nomadic behavior after the post-fledgling dependence period and (for Western European birds) typically spend their first winter in the Western Mediterranean (Ratcliffe, 1993). Only from the age of 2 years do they try to recruit into the breeding population (Kauffman et al., 2004).

Our study covered the whole of The Netherlands, which is dominated by plains, coastal lowlands and urban-farmland mosaics. During the "pesticide crash" in the 1960s (Ratcliffe, 1993; Kéry et al., in review), peregrines became extinct in The Netherlands; only in 1990 a first pair recolonized the country (van Geneijgen, 2014). Since then, the number of breeding pairs has steadily increased up to ca. 225 in 2021, but then dropped to ca. 163 until 2024 (Sovon, 2024). This decline occurred along with HPAIV outbreaks in The Netherlands

(Caliendo et al., 2024, 2025). The main source of infection for peregrine falcons and other raptors is likely by ingestion of infected prey (Caliendo et al., 2025; Cunningham et al., 2022; Günther et al., 2024).

Data acquisition and field methods

In our models, we used data from mark-resighting schemes, counts of breeding pairs, and productivity survey data.

Ever since 1993, Dutch peregrines have been intensively monitored with a ringing and resighting scheme coordinated by Werkgroep Slechtvalk Nederland (WSN) and the Dutch Ringing Scheme (Vogeltrekstation). To date, 2,807 birds have been ringed as chicks, and 74 as subadults or adults. Most birds were ringed with both alphanumeric color and metal rings (n = 2,795), while 86 birds were ringed with metal rings only. Ringed breeders were resighted during visits to breeding territories, while resightings of nonbreeders occurred throughout the country. These efforts resulted in 10.1% of ringed birds resighted at least once. In addition, ringed birds found dead were recorded in The Netherlands and abroad. In total, 15.2% of all ringed birds were recovered dead. Birds with metal rings only could not be resighted alive, because their code was too small to be read from a distance, but they could be recovered dead.

Breeding pair counts were carried out by the Sovon-Dutch Center for Field Ornithology between March and June 2010-2024. This comprised repeated visits to all known territories occupied in previous years and to potential new nesting areas in search for colonizing pairs. The resulting counts were taken as a measure of the Dutch breeding population size.

Breeding surveys were performed by the WSN in a subset of the population in the Southern Netherlands between 2010 and 2024. These included repeated visits late in the breeding season to count the number of chicks in every monitored nest. The surveys encompassed a minimum of 8 territories in 2010 and a maximum of 44 in 2021.

Analysis of population dynamics with an Integrated Population Model

We estimated demographic parameters and population dynamics by jointly analyzing the productivity (2010-2024), mark-resight-recovery (1993-2024), and population count data (2010-2024) in an Integrated Population Model (IPM; Besbeas et al. 2002, Schaub & Kéry 2022). The core of the IPM is a state-space model whose state-process model corresponds to a stochastic, stage-structured population model that reflects the life cycle of the species, and with an observation model that links the observed with the estimated number of breeding pairs. The demographic rates that drive the population are additionally informed by the productivity and the mark-resight-recovery data. Our stage-structured population model was female-based, assumed an even sex ratio, and was constructed according to a pre-breeding "census". We defined population stages considering a combination of age (1-year-old, 2-year-old, 3-year-old, 4-year-old, and 5-year-old and older individuals) and breeding status (breeder vs. nonbreeder), and immigrants. We assumed all one-year-olds (“juveniles”) are nonbreeders. We also assumed that recruitment occurs at ages 2, 3, or 4 according to probabilities that we estimated in the models, is irreversible, and that all individuals aged 5 and older were breeders. The stage-specific expected numbers of individuals in each year were given by the numbers in the preceding year and the year-specific demographic rates. This resulted in nine different population stages (eq. 1). We accommodated demographic stochasticity in the model by using Poisson distributions in one-year-old nonbreeders ("juveniles") and immigrants, and by binomial distributions for the remaining population stages (Schaub & Kéry, 2022).

$$N_{1,t+1} \sim Poisson\left(N_{B_t} * S_{1,t} * \frac{\rho_t}{2}\right),$$

$$N_{2,t+1} \sim Binomial\left(S_{2,t} * \gamma_2, N_{1,t}\right),$$

$$N_{3,t+1} \sim Binomial\left(S_{2,t} * (1-\gamma_2), N_{1,t}\right),$$

$$N_{4,t+1} \sim Binomial\left(S_{3,t} * \gamma_3, N_{3,t}\right),$$

$$N_{5,t+1} \sim Binomial\left(S_{3,t} * (1-\gamma_3), N_{3,t}\right),$$

$$N_{6,t+1} \sim Binomial\left(S_{3,t} * \gamma_3, N_{5,t}\right),$$

$$N_{7,t+1} \sim Binomial\left(S_{3,t} * (1-\gamma_3), N_{5,t}\right),$$

$$N_{8,t+1} \sim Binomial\left(S_{3,t}, N_{B,t} + N_{7,t}\right)$$

$$N_{9,t+1} \sim Poisson(\omega_t)$$

Equation 1

In Equation 1, *N* are the stage-specific population sizes, with the first subscript denoting stage class and the second one the year (see Table 1 for definitions). Symbols γ, *S*, and ω stand for recruitment and survival probabilities, and for the expected number of immigrants, respectively. Numeric subscripts in γ and *S* indicate stage classes. The number of breeders N_B is defined as the sum of the number of all stages that reproduce at time *t*:

$$N_{B_t} = N_{2,t} + N_{4,t} + N_{6,t} + N_{8,t} + N_{9,t}$$

Equation 2

All demographic parameters were estimated with full temporal (annual) random variation except for recruitment, which was estimated as constant over time, given the limited sample size and the general difficulty with which this parameter can be estimated (Schaub & Kéry 2022).

As is common in most population studies, we did not have explicit data about the number of immigrants. Therefore, we estimated it as a hidden parameter, as is common in most IPMs, taking advantage of the indirect information contained in the different data sources used in the model (Abadi et al., 2010). Here, we refer to immigrants as the yearly number of individuals that were not locally born and that bred in the population for the first time.

We related N_{B_t} to the yearly breeder counts C_t using a Poisson distribution as a way of accommodating some counting error, but which also functions as a residual error of the model (Schaub & Kéry, 2022).

$$C_t \sim Poisson(N_{B_t})$$

Equation 3

As a derived quantity, we calculated the annual number of floaters as the number of sexually mature nonbreeders, that is, the number of all nonbreeders that are two years old or older. Floaters typically act as a pool of individuals that replace dead breeders in territories, thus contributing to the stability of breeder populations by functioning as a buffer (Penteriani et al., 2011).

Submodel for productivity (ρ)

We used brood size, the number of chicks (of age 2 weeks or older) per breeding pair, as an estimate of productivity. We modelled the annual total count of fledglings (J_t) as a Poisson random variable with an expectation given by the product of the annual number of pairs monitored (M_t) and productivity rate ρ_t (Schaub & Kéry, 2022).

$$J_t \sim Poisson(M_t * \rho_t)$$

Equation 4

Submodel for survival (S) and recruitment (γ)

We jointly modelled life-encounter and dead-recovery data using a multistate capture-mark-recapture (CMR) model to estimate survival and recruitment probabilities along with live resighting and dead recovery probabilities (Burnham, 1993). We considered live resightings from within the Netherlands from February to September each year and dead recoveries from anywhere and all-year-long, with the annual divide being April 26, which was the beginning of the ringing season. Since we included recovery data from beyond the Netherlands, our survival estimate is unaffected by emigration from the study area and represents “true survival” (Burnham, 1993). Additionally, our dataset provided information about the breeding status (seen as a breeder vs. seen as a non-breeder), and the age of the individual at ringing. This information allowed us to model survival, recruitment, and live-resighting probabilities by stage class.

Multistate mark-recapture models consist of a state process, which defines the relationship between the state of an individual between years t and $t+1$, and an observation process, which relates the observation at occasion *t* to the state of an individual at time *t*. We defined six different observation states that depended on whether the individuals were alive or dead, breeders or nonbreeders, and were carrying an alphanumeric color ring or a metal ring only (see Figures S1-S2).

We defined three age classes in survival based on the peregrine life-history: one-year-olds (juveniles, S_1), two-year-olds (subadults, S_2), and individuals aged 3 and older (adults, S_3) (Faccio, 2013). For recruitment probabilities, we defined two stage classes: one for subadults (γ_2), and another for three and four-year-olds (γ_3).

The annual resighting probabilities of live ringed birds (*p*) were structured into age classes to capture the likely heterogeneity in this parameter over the life of an individual. After evaluating different age structures using goodness-of-fit testing (GoF, see Appendix S1), we retained a structure with three age classes: one for juveniles (p_1), a second for individuals aged 2 to 4 (p_2), and a third for individuals aged 5 and older. The probability to find and report a recently dead ringed individual (recovery probability, *r*), on the logit scale, was modelled as constant across age-stages, but with a linear regression on the year to accommodate likely gradual changes in recovery efforts over time.

We formulated our multistate model with a marginalized likelihood of the state-space formulation (Yackulic et al., 2020). This likelihood provides a considerable speed gain compared to the standard state-space formulation, as it avoids estimation of the discrete latent survival states (Schaub and Badia-Boher, in press).

Population projections over 10 years into the future

To gauge the longer-term impact of HPAIV, we projected the study population under two different scenarios and evaluated some key metrics of population resilience (Capdevila et al., 2020), which provides a useful framework for measuring population effects of disturbances. First, we fit our IPM with all data (i.e. 2010 – 2024), thus including the effect of the current HPAIV epizootic (2020-2024). Then, using the estimated demographic parameters, we projected population dynamics until 2034. Second, we refit the model only to the data from 2010 to 2019, to estimate parameters in the absence of any HPAIV outbreak, and we again projected the population until 2034. Our projections considered parameter uncertainty along with demographic and environmental stochasticity (Schaub & Kéry, 2022). The comparison between both scenarios allows an evaluation of key properties of a disturbance of population dynamics, i.e., of population resilience (Capdevila et al., 2020; Figure 1). First, we evaluated recovery time, i.e., the number of years required for the breeder population to again reach its size from 2021 (which was the maximum population size ever achieved, right before the most intense HPAIV outbreaks were recorded; Caliendo et al., 2025). Second, we assessed the difference between the projected breeder population size in the absence of the HPAIV outbreak (Scenario 2) and that including the outbreak years (Scenario 1) once stable growth was reached in both (i.e., 2030). This metric informs about the effect on long-term population size caused by a disturbance, or population inertia (Koons et al., 2007).

Statistical inference and model fitting

To fit models and conduct forecasts, we used Bayesian MCMC-based inference with JAGS (Plummer, 2003), run from R 4.4.2 via the package 'jagsUI' (Kellner, 2024). We ran four chains and evaluated convergence using visual assessment of traceplots and by the Brooks-Gelman-Rubin statistic (Rhat). We ran models for 80,000 iterations, discarded the first 40,000 draws as a burnin, and thinned the remainder by 1 in 40. All estimated parameters showed good mixing and had Rhat values below 1.02. Based on posterior predictive checks (Schaub & Kéry, 2022), model fit was adequate, with Bayesian *p*-values of 0.59 for the count model and 0.39 for the productivity model. The GoF results for the survival part of the model also suggested an adequate model fit (see Appendix S1). Below, we present estimates by posterior means and 95% credible intervals (CRI)in parentheses.

Results

Mean annual adult survival before the HPAIV panzootic (1994-2019) varied between 0.73 and 0.86 (Figure 2). During the panzootic period, it remained within pre-panzootic values in 2020 (0.81, 0.74-0.88), but then dropped to 0.72 (0.65-0.80) and 0.57 (0.47-0.66) in 2021 and 2022, respectively, before recovering to 0.70 (0.59-0.80) and 0.79 (0.67-0.88) in 2023 and 2024. Mean pre-panzootic survival of subadults varied between 0.58 and 0.75. During the panzootic, it declined from 0.72 (0.55-0.87) in 2020 and 2021 to 0.44 (0.16-0.70) in 2022 and 0.56 (0.36-0.75) in 2023 and then recovered to 0.73 (0.52-0.92) in 2024. Juvenile survival showed little annual variation only and fluctuated between 0.30 and 0.35 in the pre-panzootic years. There was only a vague hint of a decline during panzootic years.

Mean annual productivity rates before the HPAIV panzootic (2010-2019) varied between 1.9 and 2.2 (Figure 2). During the panzootic period, the rates were similar, oscillating between a minimum of 1.90 (1.56-2.17) in 2021 and a maximum of 2.15 (1.89-2.61) in 2023.

The estimated number of breeding pairs more than doubled from 2010 to the beginning of the panzootic, reaching 222 (200-246) in 2021. This was followed by a 25% (13%-35%) crash in just two years, reaching a minimum of 169 (150-188) pairs in 2023, with 172 (151-195) in 2024, that is, hardly any improvement (Figure 3). As for stage-specific population sizes, the number of juvenile females increased over time reaching a maximum of 77 (53-113) in 2019 and declined by 30% (18% - 66%) during the panzootic period. Similarly, floaters reached a maximum of 24 females (12-40) in 2020 and declined by 40% (37% - 76%) thereafter. The number of immigrant females was relatively constant over time, oscillating between 8 and 12 individuals on average, although with large uncertainty. However, coinciding with the decline in the breeding population in 2022, immigrant numbers grew to 20 (2-80) in 2022.

Recruitment probability was estimated at 0.67 (0-55-0.77) for two-year-olds and 0.62 (0.40-0.81) for three and four-year-olds (Figure S3). Resighting and recovery probabilities are presented in Appendix S1 and Figures S4-S5.

Fitting the model to the full data set (i.e., including the panzootic years), 10-year projections suggested a steady increase in the number of breeding pairs over the years, reaching 249 (109-482) pairs by 2034. Fitting the model instead to the reduced data set only (i.e., without the years with HPAIV outbreak), the number of breeding pairs was estimated at 205 (182-229) in 2020, 238 (167-332) in 2024 and 294 (168-508) in 2034. The estimated recovery time to the highest number of breeding pairs (2021) was 9 years on average (2031; Figure 4), although with large uncertainty. There was a probability of 23% that the 2021 numbers would not be recovered before 2034, of 57% that recovery was achieved before 2029, and of 20% of recovery between 2030 and 2034. Inertia estimates indicated that in 2030 the breeding population will have lost 21% of its size, that is, 55 breeding pairs (Figure 4), although uncertainty was again large (-127 to 235 pairs).

Discussion

The recent spread of Highly Pathogenic Avian Influenza virus HPAIV-H5N1 (2020-2024) has caused the most severe wildlife disease ever reported, but to date no demographic analyses have evaluated its effects on the dynamics of wild populations. Our results suggest that the effects of HPAIV-H5N1 outbreaks in the Dutch peregrine falcon population have been severe, with a sharp decline in adult survival and all population stages during consecutive panzootic years. Furthermore, resilience analyses predict that the population may take a decade to recover, which is concerning given the likely increase in the recurrence of HPAIV outbreaks in future years. Our findings illustrate the potentially larger population impacts caused by the new HPAIV virus and call for a global-scale conservation response.

The large drop in adult survival that we found during the HPAIV panzootic is uncommon in long-lived species. In these species, there is strong selection towards high and stable adult survival over time even in case of disturbances, given the large sensitivity of population growth rates to this parameter (i.e., “demographic buffering”, Hilde et al. 2020). As a result, declines of such magnitude often have catastrophic effects on population size, such as the quick decline in the number of breeders that we estimated over barely two years. Hence, understanding whether adult survival has been affected generally in other long-lived species affected by HPAIV is fundamental to assess the impact magnitude of the panzootic on populations. To date, we found only a single study estimating survival, in this case in colonies of northern gannets *Morus bassanus* (Lane et al., 2024). The study reported a drop of adult survival of a similar magnitude to the one we found. Besides, many monitoring schemes of affected long-lived species have reported sharp declines in breeder numbers (e.g., Falchieri et al., 2022; Avery-Gomm et al., 2024). Although no demographic studies have been performed, the rapidity of these declines and the large numbers of dead adults found in many affected populations (e.g., Knief et al., 2023; Günther et al., 2024; Rayment et al., 2025) suggests that a decline in adult survival was the main cause.

The strongest reductions in survival and breeder population size in 2022 and 2023 matched the strongest outbreaks in late winter and early spring of the same years in the Netherlands (Caliendo et al., 2024, 2025). The fact that the HPAIV-H5N1 outbreaks affected the population during consecutive years constitutes a different trend from previous HPAIV epizootics, which only generated outbreaks within single years (Kleyheeg et al., 2017). Seemingly, another new particularity of HPAIV-H5N1 is that outbreaks can extend through all seasons in many species, whilst former epizootics were limited to winters (Caliendo et al., 2025; Pohlmann et al., 2022). This epidemiological change may have considerable repercussions on population dynamics, as spring outbreaks overlap with the breeding season in many species. Energy expenditure is particularly high during breeding, which could result in higher individual vulnerability to disease, and ultimately, stronger population-level impacts (Drent & Daan, 1980). In this respect, the highest mortalities in the study population were reported already in the breeding season (March), with 93% of all sampled dead peregrines tested positive for HPAIV (n = 15, Caliendo et al., 2025). Such outbreaks in 2022 and 2023 in our population coincided with drastic drops in survival of breeders (immature and adult survival). Instead, previous winter-only outbreaks (e.g., in 2016-2017 or the first outbreak of this panzootic in the winter 2020-2021) did not coincide with noticeable declines in survival nor in the number of breeding pairs.

The combination of increased outbreak recurrence and potentially larger effects on breeder survival may be a dangerous combination for population viability. The repeated, sudden removal of large numbers of breeders may progressively slow down recovery times (Capdevila et al., 2022b). Juveniles must survive several years to reach the age of first breeding and consequently the replacement of dead breeders may take several years. In our study population, reductions in survival were accompanied by declines in the size of the floater population, which typically acts as a buffer for the breeder population. Instead, our results suggest that an increase in the number of immigrants from other populations to some degree buffered the breeder population, whose decline might have been even more drastic otherwise. Similarly, lower numbers of breeders resulted in lower numbers of fledglings in the following years. With such cascading effects, our projections revealed that the breeding population would take about a decade to recover to its former size. Importantly, recovery times could be considerably longer in other affected long-lived species with lower productivities and greater ages of first breeding (e.g., condors, albatrosses, Kozlov, 2023; Kuiken et al., 2025).

Given the likely increased recurrence of HPAIV already shown by this panzootic, it is possible that new outbreaks may impact affected populations again and slow down recovery (Pohlmann et al., 2022). Our inertia estimate suggests that the breeding population will stabilize at a size 21% lower than in the absence of the panzootic. Recurrent HPAIV outbreaks may successively lead to lower stabilizing values that are more subject to demographic stochasticity and the effects of additional threats. It will be important to monitor this and other affected populations in detail to determine whether future outbreaks will still have similar impacts on population dynamics, and how they affect population resilience.

In our study, the use of IPMs enabled the joint modelling of three key aspects of population dynamics within a unified framework: i) the retrospective impact of a disease-induced perturbation on demographic parameters and population stages, 2) the likely future response of the population, and 3) key metrics of demographic resilience. These components are rarely assessed together, and our approach thus offers a valuable and broadly applicable framework for comprehensively evaluating the effects of perturbations. Importantly, we estimated resilience metrics within the IPM by comparing future scenarios with and without the impact of HPAIV, aligning with the conceptual framework outlined by Capdevila et al. (2020). This approach contrasts with most resilience studies, which typically derive resilience metrics from population projection matrices (PPMs; Stott et al., 2011; Capdevila et al., 2022a, 2022b). In these studies, resilience estimates are hardly ever presented with their associated uncertainties, probably because these are not easy to calculate from PPMs. Instead, a notable advantage of using IPMs is that the propagation of uncertainty into the resilience estimates is straightforward. Importantly, as resilience metrics are always based on projections, their uncertainties will be inherently large, a pattern also evident in our results. Here, we focused our discussion on the means of the metrics, to adhere to standard practices in resilience studies.

The effect of HPAIV-H5N1 on juvenile survival and productivity was mild, if anything. The lack of HPAIV effects on productivity agrees with findings in other birds of prey in central and northern Europe, where this parameter was hardly affected (Günther et al., 2024). However, strong drops in productivity were found in other animal groups, suggesting that productivity effects might be taxon- or case-specific (Campagna et al., 2024; Duriez et al., 2023). In our study population, Caliendo et al. (2025) found no trace of HPAIV in unhatched eggs during the breeding season, suggesting that pre-hatching HPAIV infection was unlikely. In white-tailed sea eagles (*Haliaeetus albicilla*) in Germany, Günther et al. (2024) showed that virus prevalence in nestlings was low compared with the likely large exposure of breeding adults to HPAIV. This fact could be explained by the potential transfer of maternal antibodies to nestlings, although this has not been proved. This hypothesis could also explain the mild to nonexistent decline in juvenile survival throughout the outbreak. Interestingly, HPAIV virulence in former epizootics was found to be stronger in younger birds of some species compared to adults (Günther et al., 2024; Hill et al., 2016). This was attributed to the acquisition of an immune response in adults that survived previous outbreaks. Our more severe mortality estimates in adults could indicate the new HPAIV-

H5N1 virus escaping a potential immune response. However, further demographic and epidemiologic studies are needed to confirm this.

Crucially, this will not be the last panzootic we witness. Under ongoing global change, both spread and the impact of infectious diseases are increasing, accentuating the role of disease as a major driver of biodiversity loss. This may pose yet another challenge to the conservation of long-lived birds and mammals, which are already threatened by a number of anthropogenic factors (Rowe, 2008). In this context, a global-scale response is required. Diseases are still rarely integrated into species conservation plans, despite their growing impact. Wildlife surveillance schemes should incorporate systematic testing and sequencing to anticipate outbreaks and detect mutations, especially in species previously affected by diseases. Applied demographic research should evaluate how disease impacts differ across population stages and age classes – this would help predicting demographic impacts and targeting the most affected stages with management action (e.g., Benhaiem et al., 2018). Further efforts in applied research should prioritize building a base of evidence to identify effective management strategies and promote their implementation. For example, recent studies suggest that the removal of carcasses during HPAIV outbreaks was beneficial to limit the spread of the virus to other wild animals, pets, and ultimately to humans (Campagna et al., 2024; Rijks et al., 2022). Lastly, we should not dismiss that global change is increasing the spillover of wildlife disease to humans. Therefore, anticipating and mitigating the effects of wildlife disease should not only be seen as a measure to protect biodiversity, but also to safeguard human societies.

Acknowledgements

We are very grateful to the many volunteers who have contributed their time towards the monitoring of the Dutch peregrine population. Our special thanks also go to professionals at Sovon, Werkgroep Roofvogels Nederland, and Vogeltrekstation for sharing the data used in this study. This research was funded by the Swiss National Science Foundation grant number 310030_207603.

References

Abadi, F., Gimenez, O., Ullrich, B., Arlettaz, R., & Schaub, M. (2010). Estimation of immigration rate using integrated population models. *Journal of Applied Ecology*, 47(**2**), 393–400.

Avery-Gomm, S., Barychka, T., English, M., Ronconi R.A., Wilhelm, S.I., Rail, J.F., ..., & Wight, J. (2024). Wild bird mass mortalities in eastern Canada associated with the Highly Pathogenic Avian Influenza A(H5N1) virus, 2022. *Ecosphere*, 15, e4980.

Benhaiem, S., Marescot, L., East, M.L., Kramer-Schadt, S., Gimenez, O., Lebreton, J.D., & Hofer, H. (2018). Slow recovery from a disease epidemic in the spotted hyena, a keystone social carnivore. *Communications Biology*, 1, 201.

Besbeas, P., Freeman, S.N., Morgan, B.J., & Catchpole, E. (2002). Integrating mark–recapture–recovery and census data to estimate animal abundance and demographic parameters. *Biometrics*, 58(**3**), 540–547.

Burnham, K.P. (1993). A theory for combined analysis of ring recovery and recapture data. In Lebreton, J.D., & North, P.M. (eds), *Marked Individuals in the Study of Bird Population*, pp. (199–213). Birkhäuser Verlag, Basel, Switzerland.

Caliendo, V., Bellido Martin, B., Fouchier, R.A.M., Verdaat, H., Engelsma, M., Beerens, N., & Slaterus, R. (2025). Highly Pathogenic Avian Influenza Contributes to the Population Decline of the Peregrine Falcon (Falco peregrinus) in The Netherlands. *Viruses*, 17, 24.

Caliendo, V., Kleyheeg, E., Beerens, N., Camphuysen, K.C., Cazemier, R., Elbers, A.R., ..., & Rijks, J. M. (2024). Effect of 2020–21 and 2021–22 Highly Pathogenic Avian Influenza H5 Epidemics on Wild Birds, the Netherlands. *Emerging Infectious Diseases*, 30, 1.

Campagna, C., Uhart, M., Falabella, V., Campagna, J., Zavattieri, V., Vanstreels, R. E. T., & Lewis, M. N. (2024). Catastrophic mortality of southern elephant seals caused by H5N1 avian influenza. *Marine Mammal Science*, 40(**1**), 322–325.

Capdevila, P., Stott, I., Beger, M., & Salguero-Gómez, R. (2020). Towards a Comparative Framework of Demographic Resilience. *Trends in Ecology & Evolution*, 35(**9**), 776–786.

Capdevila, P., Stott, I., Cant, J., Beger, M., Rowlands, G., Grace, M., & Salguero-Gómez, R. (2022a). Life history mediates the trade-offs among different components of demographic resilience. *Ecology Letters*, 25, 1566-1679.

Capdevila, P., Noviello, N., McRae, L., Freeman, R., & Clements, C. F. (2022b). Global patterns of resilience decline in vertebrate populations. *Ecology Letters*, 25(**1**), 240-251.

Cunningham, E., Gamble, A., Hart, T., Humphreys, E., Philip, E., Tyler, G., & Wood, M. (2022). The incursion of Highly Pathogenic Avian Influenza (HPAI) into North Atlantic seabird populations: An interim report from the 15th International Seabird Group conference. *Seabird Journal*, 34, 67–73.

Daszak, P., Cunningham, A.A., & Hyatt, A.D. (2000). Emerging Infectious Diseases of Wildlife—Threats to Biodiversity and Human Health. *Science*, 287(**5452**), 443–449.

Dobson, A., & Foufopoulos, J. (2001). Emerging infectious pathogens of wildlife. *Philosophical Transactions of the Royal Society of London. Series B: Biological Sciences*, 356(**1411**), 1001–1012.

Drent, R.H., & Daan, S. (1980). The Prudent Parent: Energetic Adjustments in Avian Breeding. *Ardea*, 68, 225–252.

Duriez, O., Sassi, Y., Gall-Ladevèze, C. L., Giraud, L., Straughan, R., Dauverné, L., ..., & Loc'h, G. L. (2023). Highly pathogenic avian influenza affects vultures' movements and breeding output. *Current Biology*, 33, 3766-3774.

Faccio, S.D. (2013). Movement Patterns, Natal Dispersal, and Survival of Peregrine Falcons Banded in New England. *Journal of Raptor Research*, 47(3), 246–261.

Falchieri, M., Reid, S.M., Ross, C.R., James, J., Byrne, A.M.P., Zamfir, M., ..., & Miles, W. (2022). Shift in HPAI infection dynamics causes significant losses in seabird populations across Great Britain. *Veterinary Record*, 191(7), 294-296.

Günther, A., Krone, O., Globig, A., Pohlmann, A., King, J., Fast, C., ..., & Beer, M. (2024b). Avian raptors are indicator species and victims of high pathogenicity avian influenza virus HPAIV H5N1 (clade 2.3.4.4b) in Germany. *Scientific Reports*, 14(**1**), 28779.

Hilde, C.H., Gamelon, M., Sæther, B.E., Gaillard, J.M., Yoccoz, N.G., & Pélabon, C. (2020). The Demographic Buffering Hypothesis: Evidence and Challenges. *Trends in Ecology and Evolution*, 35(6), 523-538.

Hill, S.C., Manvell, R.J., Schulenburg, B., Shell, W., Wikramaratna, P.S., Perrins, C., Sheldon, B. C., ..., & Pybus, O.G. (2016). Antibody responses to avian influenza viruses in wild birds broaden with age. *Proceedings. Biological Sciences*, 283, 20162159.

Järås, T. (2023). Expertens larm: Pilgrimsfalkar dör av fågelinfluensa. *Sveriges Radio*. Acessed 29 April 2025. https://www.sverigesradio.se/artikel/expertens-larm-pilgrimsfalkar-dor-av-fagelinfluensa

Kauffman, M.J., Pollock, J.F., & Walton, B. (2004). Spatial Structure, Dispersal, and Management of a Recovering Raptor Population. *The American Naturalist*, 164(**5**), 582–597.

Kellner, K. (2024). jagsUI: A wrapper around’rjags’ to streamline’JAGS’analyses (Version 1.6.2). Retrieved from: https://cran.r-project.org/web/packages/jagsUI/index.html

Klaassen, M., & Wille, M. (2023). The plight and role of wild birds in the current bird flu panzootic. *Nature Ecology & Evolution*, 7(**10**), 1541-1542.

Kleyheeg, E., Slaterus, R., Bodewes, R., Rijks, J.M., Spierenburg, M.A.H., Beerens, N., ..., & van der Jeugd, H. P. (2017). Deaths among Wild Birds during Highly Pathogenic Avian Influenza A(H5N8) Virus Outbreak, the Netherlands. *Emerging Infectious Diseases*, 23(**12**), 2050–2054.

Knief, U., Bregnballe, T., Alfarwi, I., Ballmann, M.Z., Brenninkmeijer, A., Bzoma, S., ..., & Courtens, W. Highly pathogenic avian influenza causes mass mortality in Sandwich Tern Thalasseus sandvicensis breeding colonies across northwestern Europe. *Bird Conservation International*, 34, e6, 1-11.

Koons, D.N., Holmes, R.R., & Grand, J.B. (2007). Population Inertia and Its Sensitivity to Changes in Vital Rates and Population Structure. *Ecology*, 88(**11**), 2857–2867.

Kozlov, M. (2023). United States to vaccinate birds against avian flu for first time. *Nature*, 618, 220-221.

Kuiken, T., Vanstreels, R., Banyard, A., Begeman, L., Breed, A., Dewar, M., ..., & Wille, M. (2025). Emergence, spread, and impact of high pathogenicity avian influenza H5 in wild birds and mammals of South America and Antarctica, October 2022 to March 2024. *EcoEvoRxiv*. https://doi.org/10.32942/X2P35R .

Lambertucci, S.A., Santangeli, A., & Plaza, P.I. (2025). The threat of avian influenza H5N1 looms over global biodiversity. Nature Reviews Biodiversity, 1, 7–9.

Lane, J.V., Jeglinski, J.W.E., Avery-Gomm, S., Ballstaedt, E., Banyard, A C., Barychka, T., Brown, I. H., ..., & Votier, S.C. (2024). High pathogenicity avian influenza (H5N1) in Northern Gannets (Morus bassanus): Global spread, clinical signs and demographic consequences. *Ibis*, 166(**2**), 633–650.

Molini, U., Yabe, J., Meki, I.K., Ouled Ahmed Ben Ali, H., Settypalli, T.B.K., Datta, S., ..., & Dundon, W.G. (2023). Highly pathogenic avian influenza H5N1 virus outbreak among

Cape cormorants (Phalacrocorax capensis) in Namibia, 2022. *Emerging Microbes & Infections*, 12(**1**), 2167610.

Muñoz, G., Ulloa, M., Alegría, R., Quezada, B., Bennett, B., Enciso, N., ..., & Araya, H. (2024). Stranding and mass mortality in humboldt penguins (Spheniscus humboldti), associated to HPAIV H5N1 outbreak in Chile. *Preventive Veterinary Medicine*, 227, 106206.

Newton, I. (1979). *Population ecology of raptors*. Buteo Books, Vermillion, SD.

Penteriani, V., Ferrer, M., & Delgado, M. del M. (2011). Floater strategies and dynamics in birds, and their importance in conservation biology: Towards an understanding of nonbreeders in avian populations. *Animal Conservation*, 14(**3**), 233-241.

Plaza, P.I., Gamarra-Toledo, V., Euguí, J.R., & Lambertucci, S.A. (2024a). Recent Changes in Patterns of Mammal Infection with Highly Pathogenic Avian Influenza A(H5N1) Virus Worldwide. *Emerging Infectious Diseases*, 30(**3**), 444–452.

Plaza, P.I., Gamarra-Toledo, V., Euguí, J.R., Rosciano, N., & Lambertucci, S.A. (2024b). Pacific and Atlantic sea lion mortality caused by highly pathogenic Avian Influenza A (H5N1) in South America. *Travel Medicine and Infectious Disease*, 59, 102712.

Plummer, M. (2003). JAGS: A program for analysis of Bayesian graphical models using Gibbs sampling. *Proceedings of the 3rd International Workshop on Distributed Statistical Computing*. Technische Universität Wien, Vienna.

Pohlmann, A., King, J., Fusaro, A., Zecchin, B., Banyard, A.C., Brown, I.H., ..., & Harder, T. (2022). Has Epizootic Become Enzootic? Evidence for a Fundamental Change in the Infection Dynamics of Highly Pathogenic Avian Influenza in Europe, 2021. *mBio*, 13(**4**), e00609-22.

Pohlmann, A., Stejskal, O., King, J., Bouwhuis, S., Packmor, F., Ballstaedt, E., ..., & Harder, T. (2023). Mass mortality among colony-breeding seabirds in the German Wadden Sea in 2022 due to distinct genotypes of HPAIV H5N1 clade 2.3.4.4b. *Journal of General Virology*, 104(**4**), 001834.

Ratcliffe, D. (1993). *The peregrine falcon*. T & A D Poyser, London.

Rayment, K.M., Franzen-Klein, D., Kurimo-Beechuk, E., Poulson, R.L., Brown, J., Mendoza, K., ..., & Hall, V. (2025). Exposure and survival of wild raptors during the 2022–2023 highly pathogenic influenza a virus outbreak. *Scientific Reports*, 15(1), 6574.

Rijks, J.M., Leopold, M.F., Kühn, S., Veld, R. in 't, Schenk, F., Brenninkmeijer, A., ..., & Beerens, N. (2022). Mass Mortality Caused by Highly Pathogenic Influenza A(H5N1) Virus in Sandwich Terns, the Netherlands, 2022. *Emerging Infectious Diseases*, 28(**12**), 2538–2542.

Rowe, C. L. (2008). “The Calamity of So Long Life”: Life Histories, Contaminants, and Potential Emerging Threats to Long-lived Vertebrates. *BioScience*, 58(**7**), 623–631.

Sæther, B.E., & Bakke, Ø. (2000). Avian life history variation and contribution of demographic traits to the population growth rate. *Ecology*, 81(**3**), 642–653.

Schaub, M., & Kéry, M. (2022). Integrated population models: Theory and ecological applications with R and JAGS. Academic Press.

Shi, J., Zeng, X., Cui, P., Yan, C., & Chen, H. (2023). Alarming situation of emerging H5 and H7 avian influenza and effective control strategies. *Emerging Microbes & Infections*, 12(**1**), 2155072.

Sovon (2024). Peregrine Falcon. Accessed on April 11, 2025. https://stats.sovon.nl/stats/soort/3200/?language=english

Stott, I., Towlney, S., & Hodgson, D.J. (2011). A framework for studying transient dynamics of population projection matrix models. *Ecology letters*, 14, 959-970.

Sundvall, E (2024). Raportti maakotkan, muuttohaukan, tunturihaukan sekë poronhoitoalueen merikotkan pesinnöistä vuonna 2024. *Metsähallitus*, Helsinki.

van Geneijgen, P. (2014). Herkomst en populatiedynamiek van broedende Slechtvalken Falco peregrinus in Nederland: De eerste 24 jaar van een populatie in opbouw 5. *De Takkeling*, 22(**2**), 148–162.

van Meerendonk, W.W.A. (2023). De Slechtvalk Falco peregrinus als broedvogel in Zoetermeer. *De Takkeling*, 31(**3**), 259–272.

Yackulic, C.B., Dodrill, M., Dzul, M., Sanderlin, J.S., & Reid, J.A. (2020). A need for speed in Bayesian population models: A practical guide to marginalizing and recovering discrete latent states. *Ecological Applications*, 30(**5**), e02112.

Table and Figure Legends

Table 1. Definition of the symbols for the stage-specific population sizes used in the Integrated Population Model.

Figure 1. Schematic showing recovery time, disturbance duration, and inertia in a hypothetical population affected by a disturbance. The thick blue line represents the trajectory of a population affected by a disturbance event. The dashed black line represents the size trajectory of the same population not affected by the disturbance.

Figure 2. Stage-specific survival and productivity estimates over the years. Points indicate means and whiskers indicate 95% credible intervals. The dashed rectangle with the lightning symbol encompasses the years where HPAI-H5N1 outbreaks were reported in the study population.

Figure 3. Stage-specific population sizes over the years. Thick lines indicate mean values, and grey shaded areas indicate 95% credible intervals. The dashed rectangle with the lightning symbol encompasses the years where HPAI-H5N1 outbreaks were reported in the study population.

Figure 4. Mean numbers of breeding pairs over the years in models including years with HPAI-H5N1 outbreaks (2010-2024) and not including them (2010-2019), plus projections until 2034. The annotated values refer to the duration of the HPAI perturbation (T), the median recovery time (R), and median interia (I).

Table 1

Symbol	Definition
$\boldsymbol{N_{1,t}}$	Locally born, 1-year-old nonbreeders at year *t*
$\boldsymbol{N_{2,t}}$	Locally born, 2-year-old first-time breeders at year *t*
$\boldsymbol{N_{3,t}}$	Locally born 2-year-old nonbreeders at year *t*
$\boldsymbol{N_{4,t}}$	Locally born 3-year-old first-time breeders at year *t*
$\boldsymbol{N_{5,t}}$	Locally born 3-year-old nonbreeders at year *t*
$\boldsymbol{N_{6,t}}$	Locally born 4-year-old first-time breeders at year *t*
$\boldsymbol{N_{7,t}}$	Locally born 4-year-old nonbreeders at year *t*
$\boldsymbol{N_{8,t}}$	Experienced breeders at year *t*
$\boldsymbol{N_{9,t}}$	Immigrant first-time breeders at year *t*

Figure 1

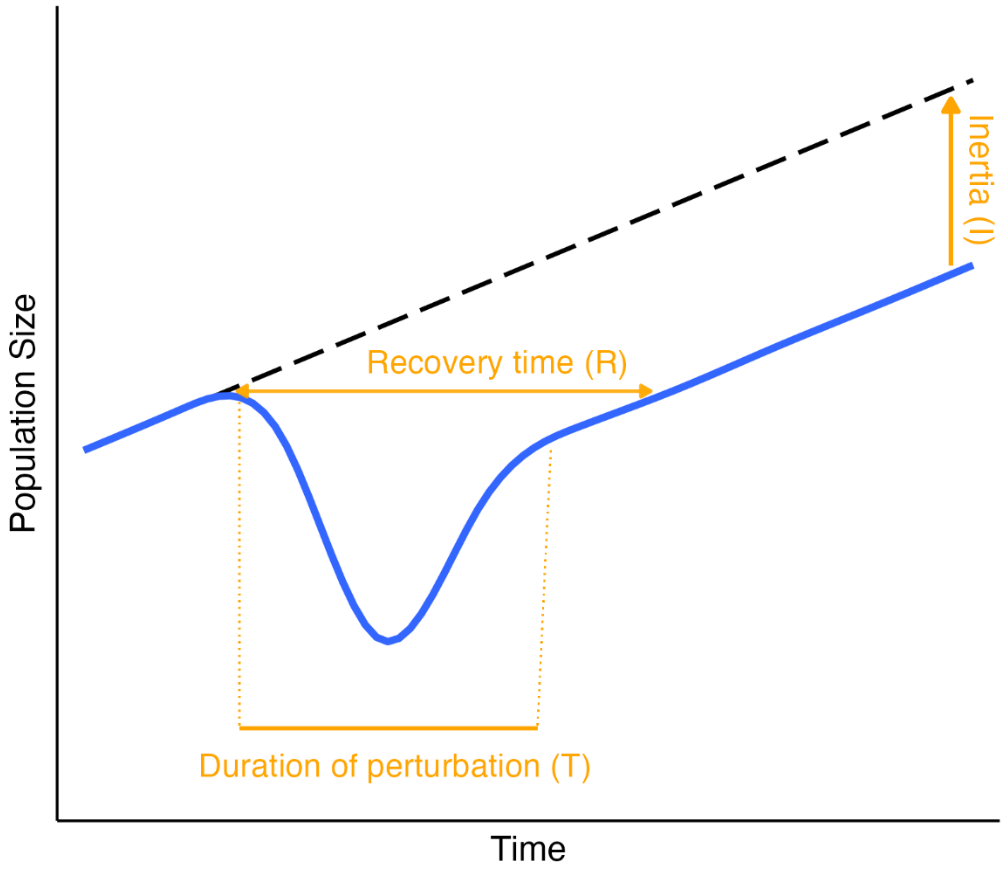
Population Size
Recovery time (R)
Inertia (I)
Duration of perturbation (T)
Time

Figure 2

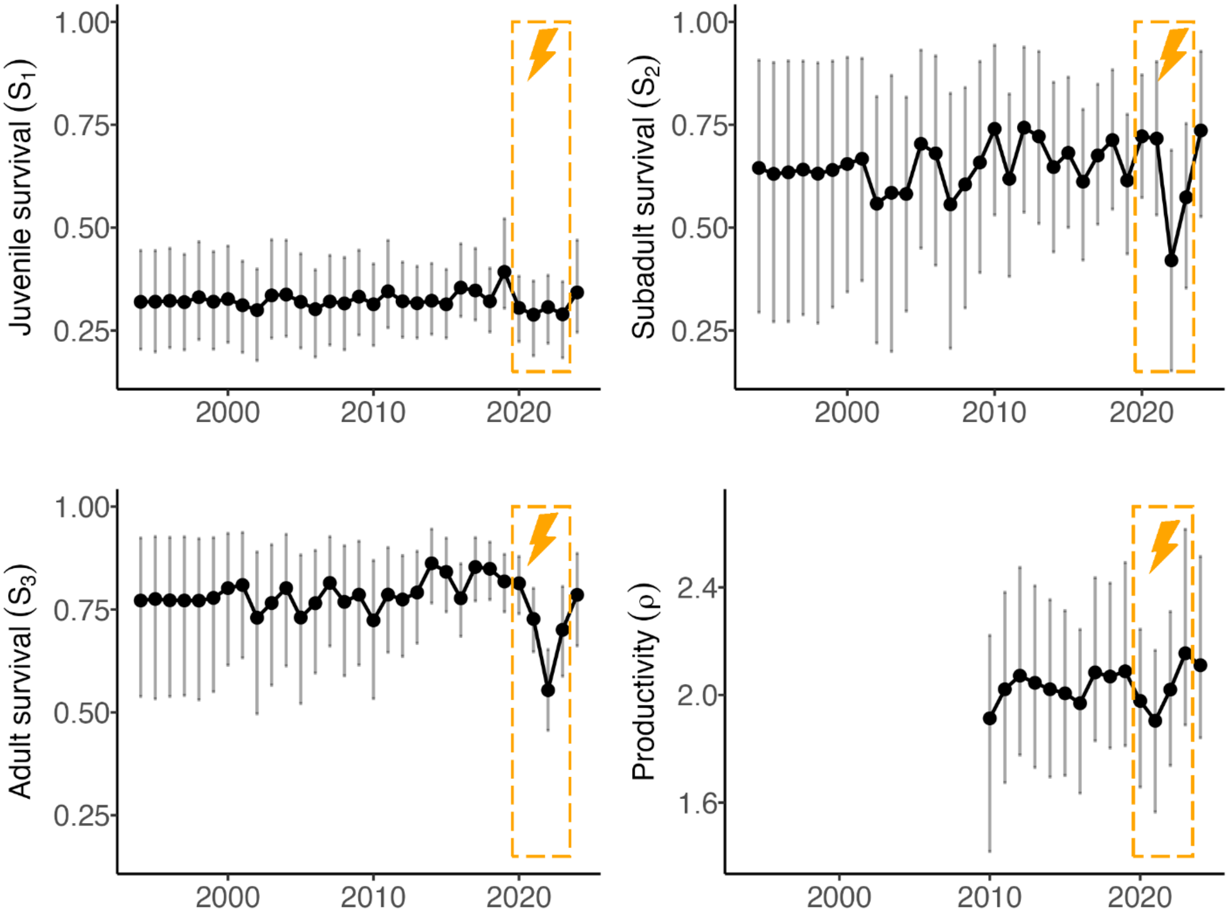
Juvenile survival (S_1)
Subadult survival (S_2)
Adult survival (S_3)
Productivity (ρ)
1.00
0.75
0.50
0.25
2.4
2.0
1.6
2000
2010
2020

Figure 3

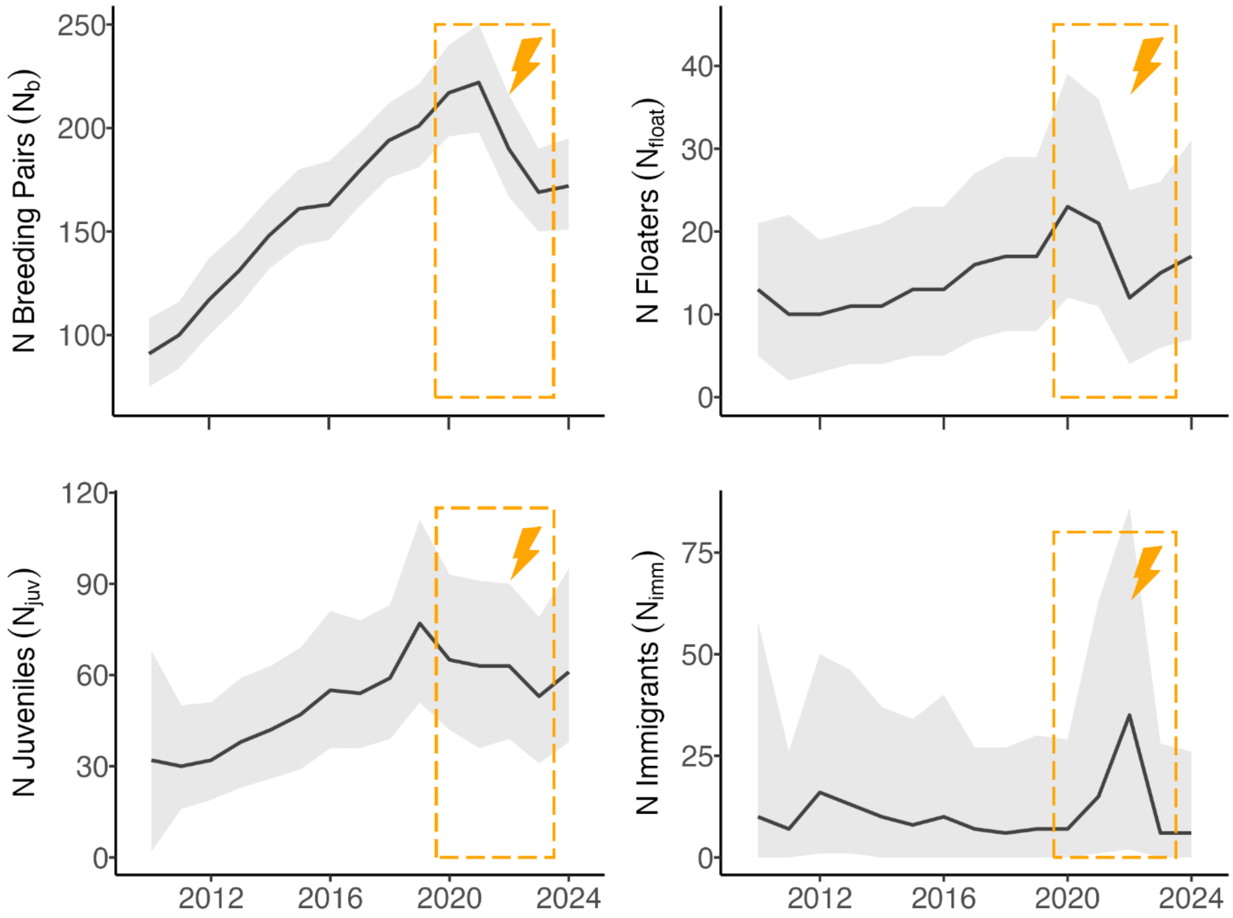
N Breeding Pairs (N_b)
250
200
150
100
N Floaters (N_{float})
40
30
20
10
0
N Juveniles (N_{juv})
120
90
60
30
0
2012
2016
2020
2024
N Immigrants (N_{imm})
75
50
25
0
2012
2016
2020
2024

Figure 4

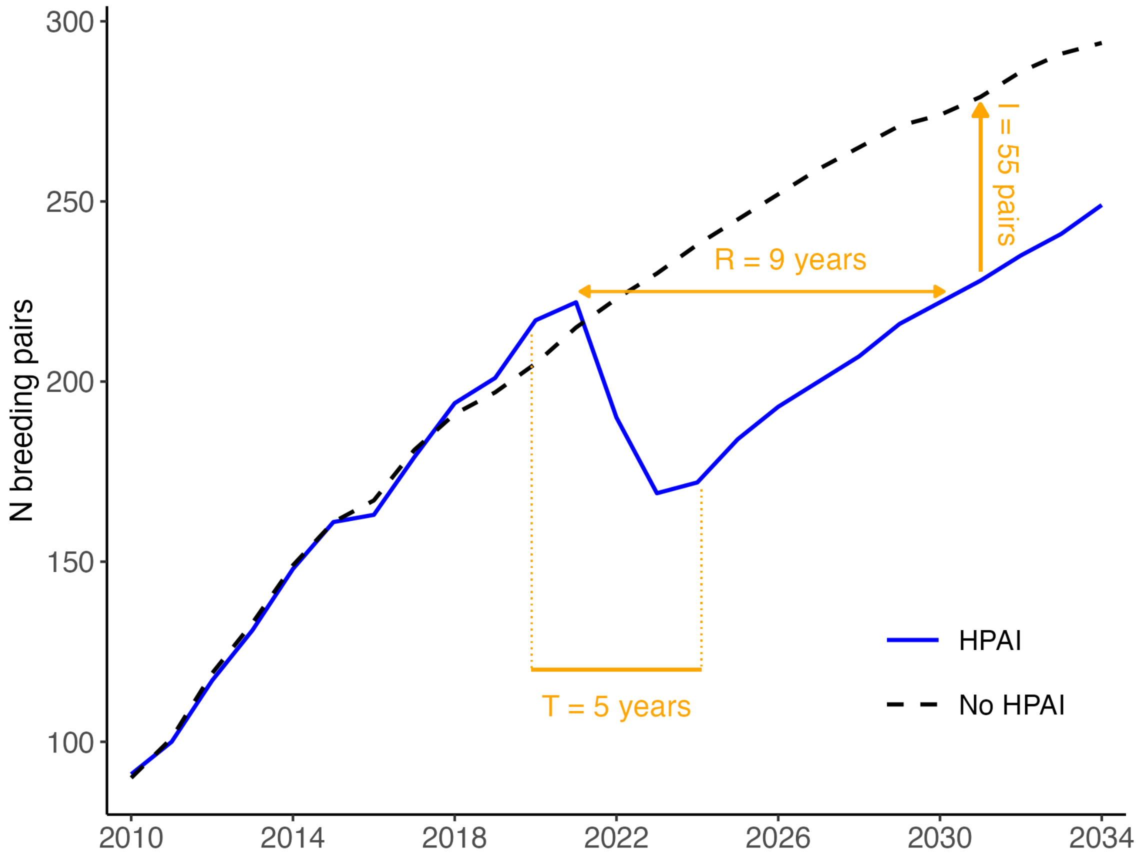
N breeding pairs
300
250
200
150
100
2010
2014
2018
2022
2026
2030
2034
R = 9 years
I = 55 pairs
T = 5 years
HPAI
No HPAI

Appendix S1

Methods

Modelling the age-structured resighting probabilities of live ringed birds (parameter *p* in our model)

The annual resighting probabilities of live ringed birds (p) were structured into age classes to capture the likely heterogeneity in this parameter over the life of an individual. Heterogeneity is mainly due to the fact that resighting effort is typically directed at breeding individuals, so younger birds that are not yet breeding have a lower chance of being resighted. In peregrine falcon studies, two resighting probabilities are typically modelled: one for juveniles, and another for older birds (Schaub & Kéry, 2022). However, for our data, this led to a significant result of the resighting heterogeneity test of the Jolly-Move Goodness-of-Fit (GoF) test for mark-recapture data ($p < 0.001$; Pradel et al., 2005). An alternative structure matching the age classes with those of survival probabilities (juveniles vs. subadults vs. adults) also resulted in a violation of the GoF test ($p = 0.01$). Finally, we tested a third structure for resighting that had the same age structure as our recruitment parameter, with p_1 for juveniles (all nonbreeders), p_2 for individuals aged 2 to 4 (where a fraction of the individuals is already recruited and some may still remain as nonbreeders), and p_3 for individuals aged 5 and older (when everyone is a breeder). This resulted in an acceptable result of the GoF test ($p = 0.17$), and hence we retained this structure for resighting probability. All other Jolly-Move GoF tests (trap-response, survival heterogeneity) showed nonsignificant results.

Results

Mean resighting probabilities of live individuals over the study period were estimated at 0.06 (0.04-0.09) for juveniles, 0.16 (0.12-0.20) for two-, three-, and four-year-olds, and 0.43 (0.36-0.51) for five-year-old and older birds respectively. We found little variation over time in all live resighting probabilities for most of the study period, although they generally tended to increase in later years (2019-2024, Figure S4). Recovery probabilities of dead individuals increased over time, with a minimum of 0.07 (0.04-0.11) in 1994 and a maximum of 0.20 (0.18-0.23) in 2024 (Figure S5). The slope parameter of the recovery linear regression, β, was estimated at 0.37 (0.19-0.56) and the probability that the recovery probabilities increased over time was 1.

References

Pradel, R., Gimenez, O., & Lebreton, J.D. (2005). Principles and interest of GOF tests for multistate capture–recapture models. Animal Biodiversity and Conservation, 28(2), 189–204.

Figure S1

	NB2	**NB1**	**B2**	**B1**	**D**	**LD**
NB2	$S_{a,t} * (1 - \gamma_a)$	0	$S_{a,t} * \gamma_a$	0	$1 - S_{a,t}$	0
NB1	0	$S_{a,t} * (1 - \gamma_a)$	0	$S_{a,t} * \gamma_a$	$1 - S_{a,t}$	0
B2	0	0	$S_{a,t}$	0	$1 - S_{a,t}$	0
B1	0	0	0	$S_{a,t}$	$1 - S_{a,t}$	0
D	0	0	0	0	0	1
LD	0	0	0	0	0	1

Figure S1. State-transition matrix in the multistate model. Rows denote states in year *t* and columns states in year *t*+1. State codes NB2 and NB1, respectively, stand for alive NonBreeders with 2 rings (alphanumeric color ring and metal ring) and with 1 (metal) ring only. B2 and B1 stand for an alive Breeder with 2 rings and 1 ring, respectively. Code D is “recently Dead” and code LD is “Long-Dead”. The formulation with two dead states is necessary to model the recovery process of dead individuals and restricts the recovery process to the year of death. Parameters γ and *S* denote recruitment and survival, respectively. Subscripts *a* and *t* indicate age class and year, respectively.

Figure S2

	sNB2	**sNB1**	**sB2**	**sB1**	**sD**	**NS**
NB2	$p_{a,t}$	0	0	0	0	$1 - p_{a,t}$
NB1	0	0	0	0	0	1
B2	0	0	$p_{a,t}$	0	0	$1 - p_{a,t}$
B1	0	0	0	0	0	1
D	0	0	0	0	r_t	$1 - r_t$
LD	0	0	0	0	0	1

Figure S2. Observation matrix in the multistate model. Rows indicate states and columns indicate observations in year *t*. State codes have the same meaning as in Figure S1 and lower case “s” in front of the observation states means “seen as”. Observation code NS means 'Not Seen'. Parameters *p* and *r* stand for resighting and recovery probabilities, respectively. Subscripts *a* and *t* indicate age class and year respectively.

Figure S3

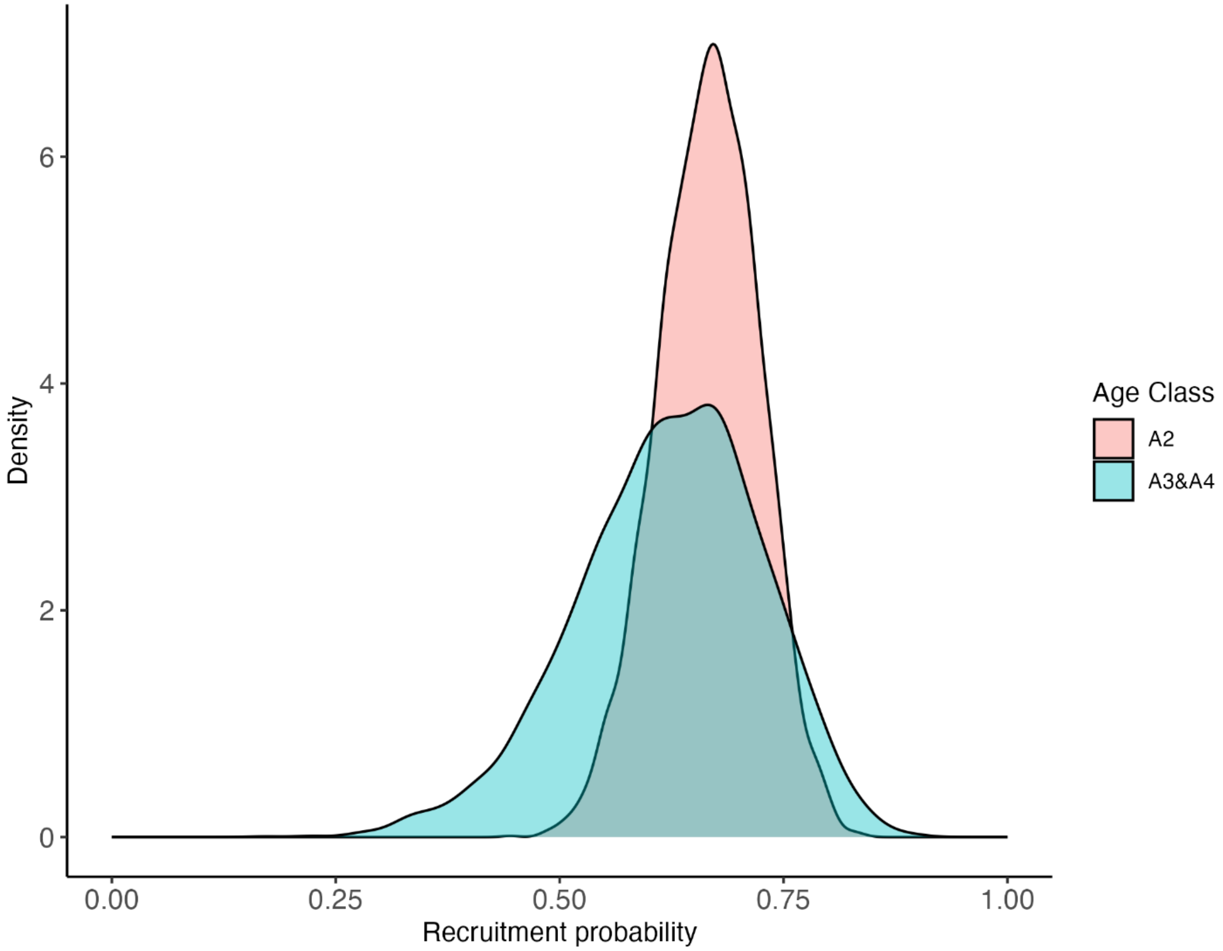

Figure S3. Posterior distributions of the probabilities of recruitment to the breeding population for two-year-olds or subadults (“A2”) and adults of ages 3 and 4 (“A3&A4”). Recruitment probabilities for individuals aged 1 were set to 0, and for adults aged 5 and older they were set to 1.

Figure S4

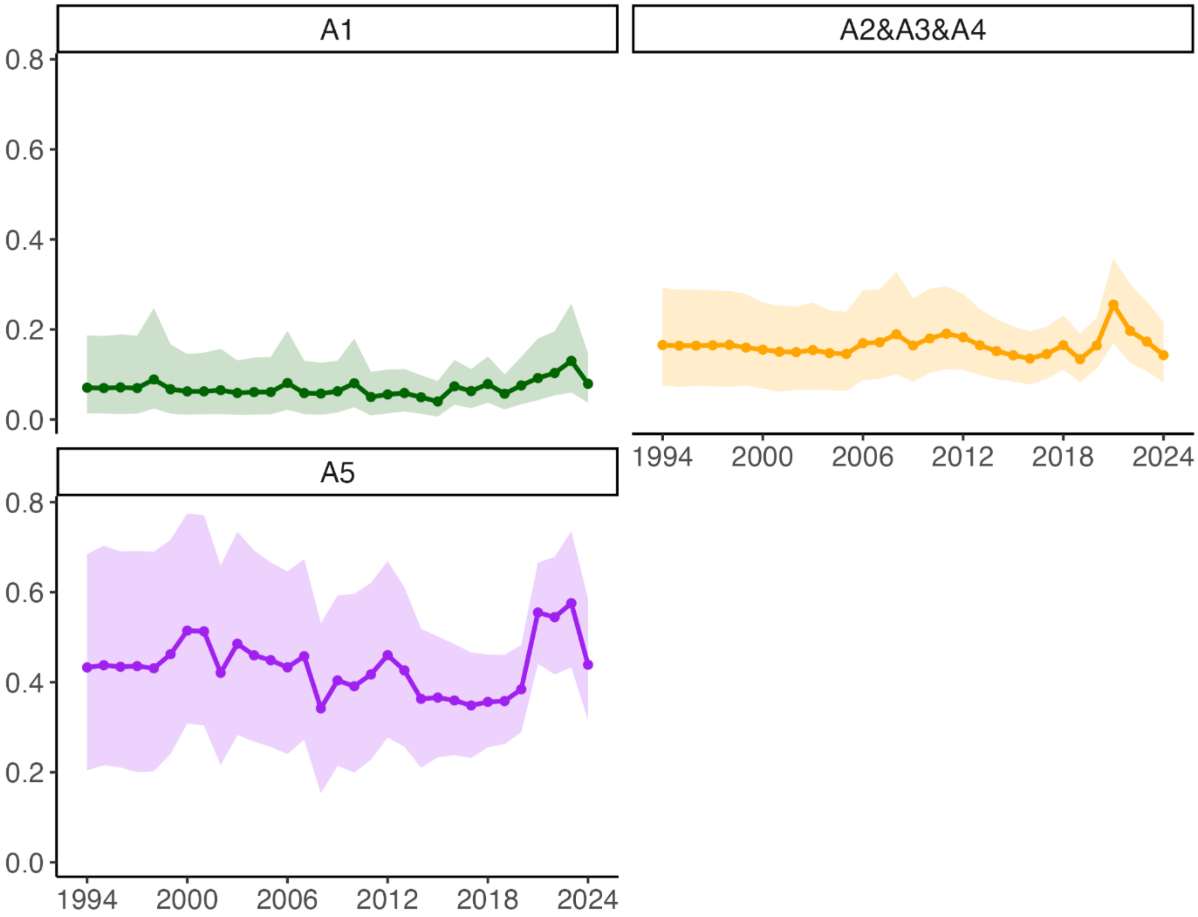

Figure S4. Yearly resighting probabilities of live individuals of age 1 (“A1”), ages 2, 3, and 4 (“A2&A3&A4”), and ages 5 and older (“A5”). Points indicate yearly means and shaded areas indicate 95% credible intervals.

Figure S5

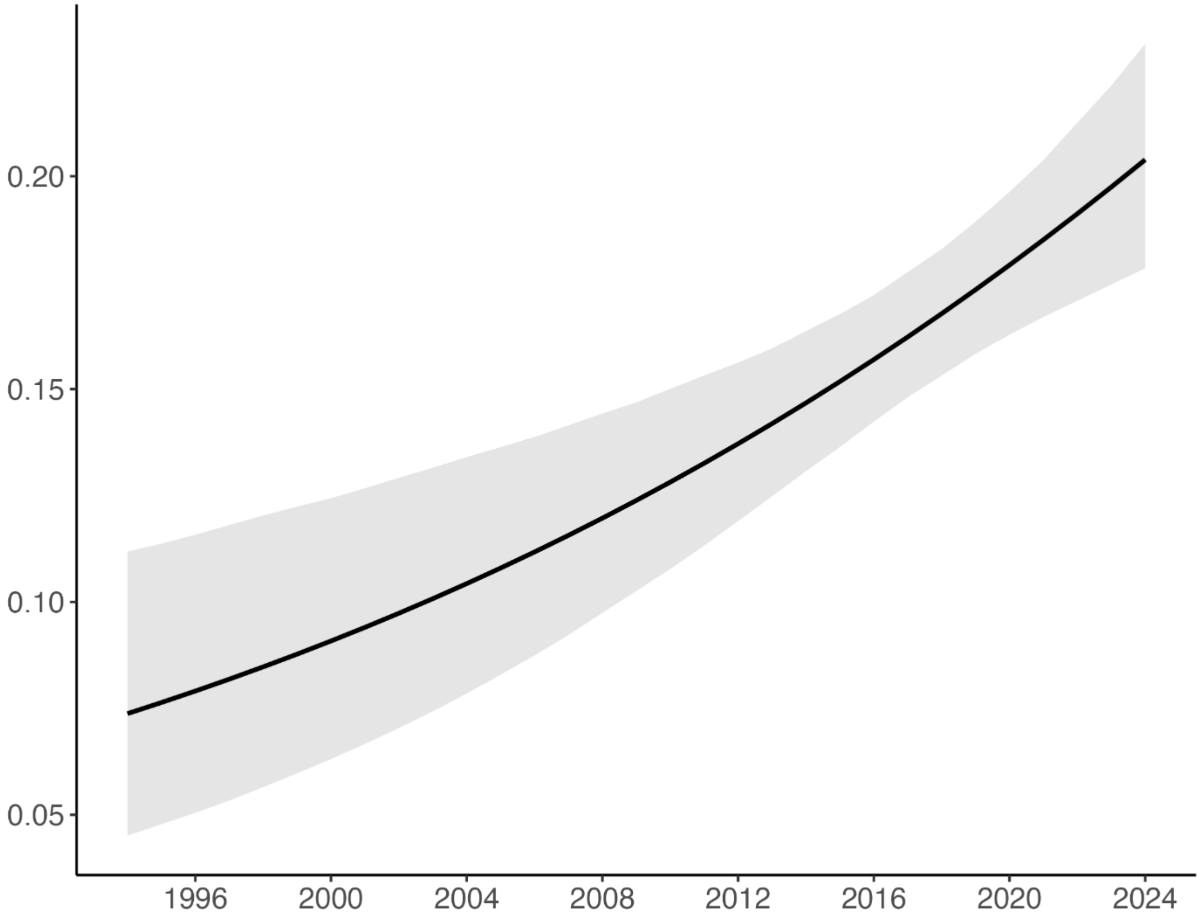

Figure S5. Yearly recovery probabilities of dead individuals. The black line indicates the mean and the shaded area indicates 95% credible intervals.